

Supporting Information

High-Resistance-State Tunneling in 25 nm $\text{TiO}_x/\text{Y-Doped HfO}_2/\text{Pt}$ Nanocrossbar Ferroelectric Tunnel Junctions

Zhongzheng Sun,^a Yoshiko Nakamura,^b Kazuki Okamoto,^b Seiichiro Izawa,^a Hiroshi Funakubo^b and Yutaka Majima*^a

* Corresponding author

^a Materials and Structures Laboratory, Institute of Integrated Research, Institute of Science Tokyo,
Yokohama, 226-8503, Japan

E-mail: majima@msl.titech.ac.jp

^b School of Materials and Chemical Technology, Institute of Science Tokyo,
Yokohama, 226-8503, Japan

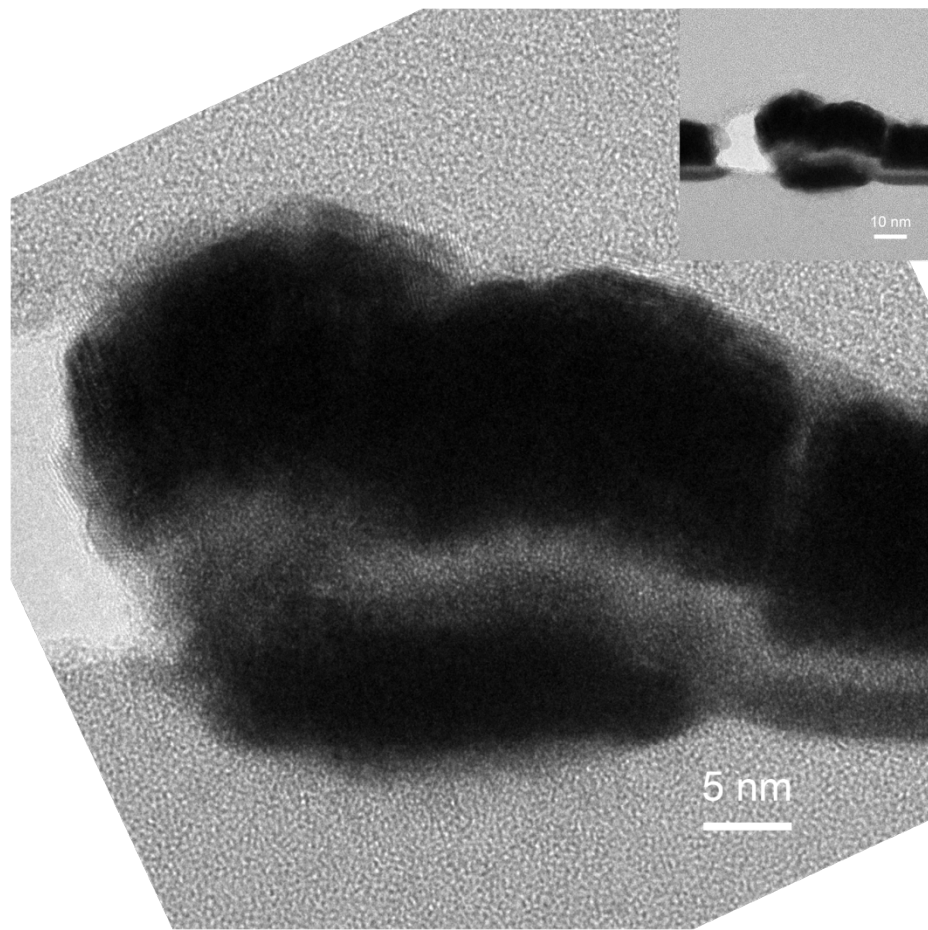


Figure S1. Bright-field transmission electron microscopy (BF-TEM) image of the cross-sectional Ti/TiO_x/YHO₇/Pt stack on a SiO₂/Si substrate corresponding to the sample shown in Fig. 2(b).

The wide-view TEM image is provided in the top-right inset. During FIB thinning, the left side fractured, resulting in distortion visible in the inset. In the undistorted right half, the TEM image clearly reveals the layered structure corresponding to the false-colored cross-sectional FE-SEM image shown in Figure 2b. The dark upper and lower regions correspond to Pt electrodes, and the bright TiO_x (upper) and a slightly darker YHO₇ (lower)s are observed between them. The YHO₇ layer (film exhibits uniform thickness and intimate contact with both the semi-circular Pt bottom electrode and the Ti/TiO_x top electrode, demonstrating successful conformal deposition of the ultrathin ferroelectric layer.

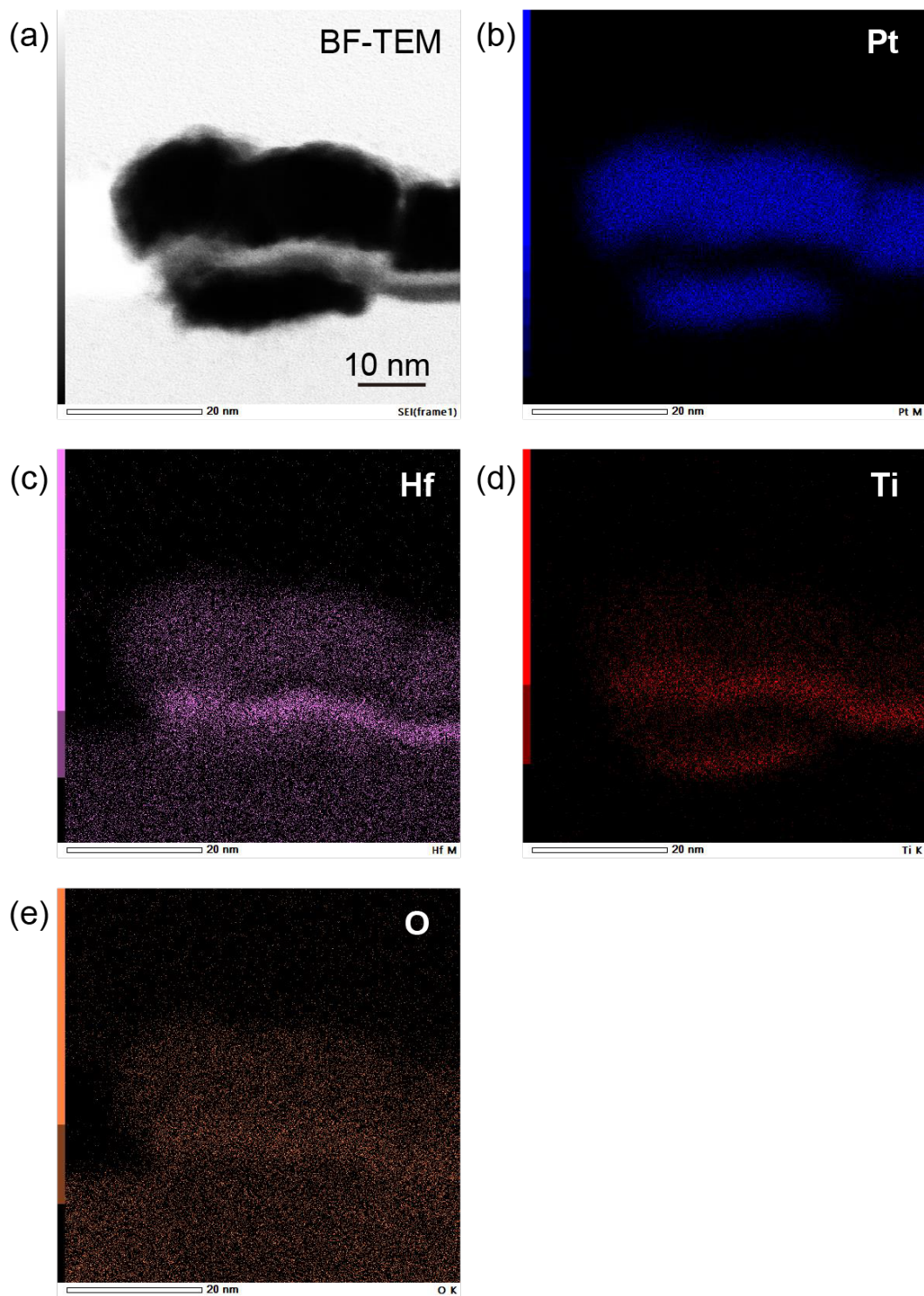


Figure S2. Cross-sectional BF-TEM image and energy-dispersive X-ray spectroscopy (EDS) elemental mapping of the Ti/TiO_x/YHO₇/Pt structure.

Elemental maps of (b) Pt (blue), (c) Hf (purple), (d) Ti (red), and (e) O (orange) obtained from (a) BF-TEM image, which is the same cross-sectional region shown in Figure S1. The oxygen map confirms the oxidation of Ti, and the Hf map indicates the uniform formation of the YHO₇ layer. The distinct elemental distributions confirm the Ti/TiO_x/YHO₇/Pt multilayer configuration and corroborate the cross-sectional morphology observed in the FE-SEM image of Figure 2b.

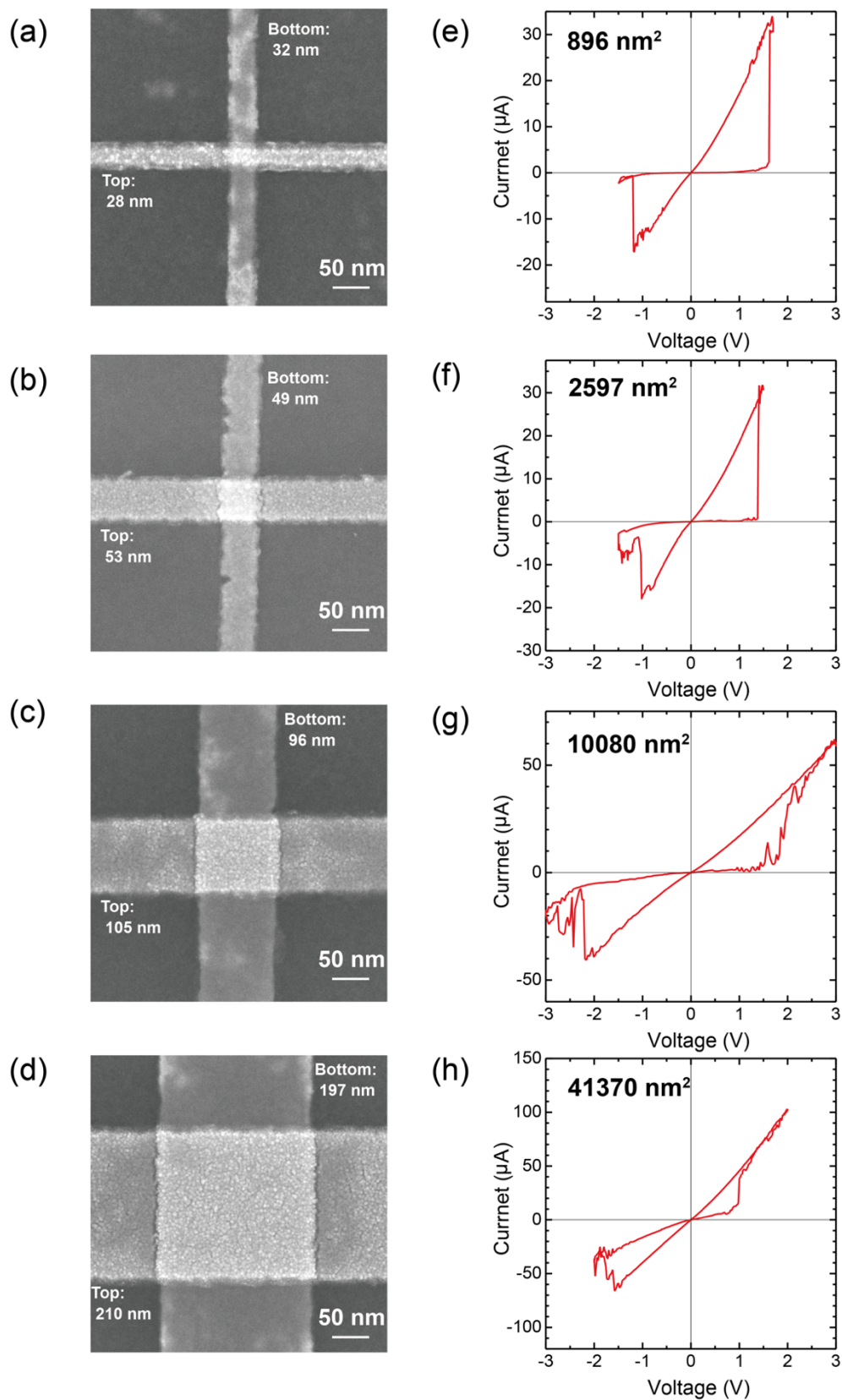


Figure S3. Typical SEM images of nanocrossbar FTJ with 3 nm YHO₇ for junction area of (a) 896, (b) 2,597, (c) 10,080, and (d) 41,370 nm². Corresponding representative I-V hysteresis loops for junction area of (e) 896, (f) 2,597, (g) 10,080, and (h) 41,370 nm² at room temperature (300 K).

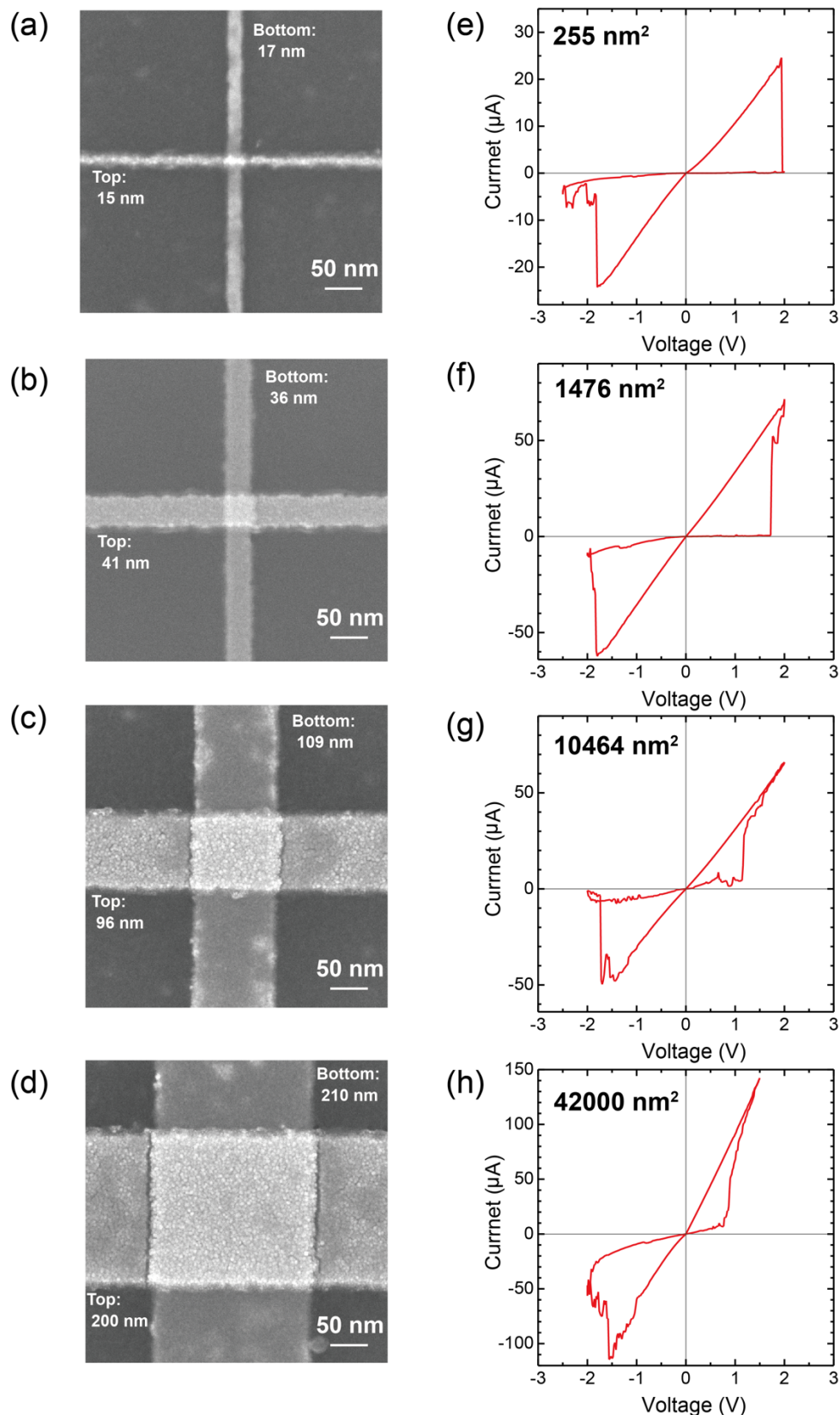


Figure S4. Typical SEM images of nanocrossbar FTJ with 2 nm YHO₇ for junction area of (a) 255, (b) 1,476, (c) 10,464, and (d) 42,000 nm^2 . Corresponding representative I-V hysteresis loops for junction area of (e) 255, (f) 1,476, (g) 10,464, and (h) 42,000 nm^2 at room temperature (300 K).

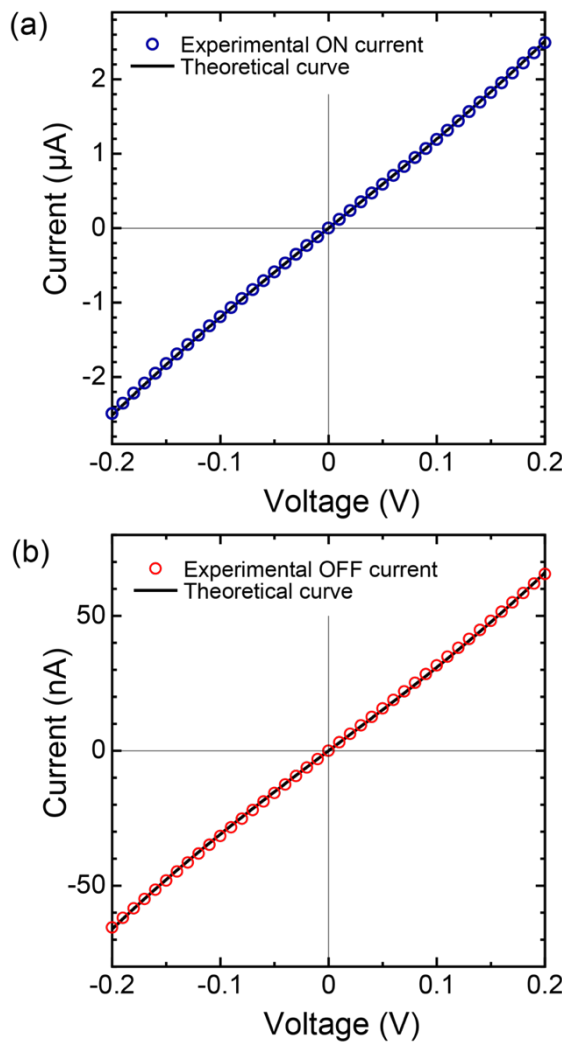


Figure S5. Fitting of the experimental I - V characteristics using the Simmons direct tunneling model.

(a) Low-resistance-state (LRS: ON-state; blue open circles) and (b) High-resistance-state (HRS: OFF-state; red open circles) experimental I - V characteristics of the Ti/TiO_x/YHO₇/Pt nanocrossbar FTJ (junction area: 896 nm², YHO₇ thickness: 3 nm) at room temperature (300 K) fitted with the theoretical curves (solid lines) calculated using the Simmons direct tunneling model in the intermediate voltage range ($V < \phi/e$).¹ The excellent agreement between the experimental and theoretical curves for both LRS and HRS confirms that electron transport in both resistance states is governed by direct tunneling through the ultrathin tunneling barrier consisting of the TiO_x depletion layer and the YHO₇ layer.

The current at the intermediate voltage range is given by

$$I(V) \propto \frac{1}{d^2} \left[\left(\phi - \frac{eV}{2} \right) \exp \left(-\frac{4\pi d}{h} \sqrt{2m^*} \sqrt{\phi - \frac{eV}{2}} \right) - \left(\phi + \frac{eV}{2} \right) \exp \left(-\frac{4\pi d}{h} \sqrt{2m^*} \sqrt{\phi + \frac{eV}{2}} \right) \right]$$

where m^* is the effective mass of the electron, e is the elementary charge, h is Planck's constant, d is the barrier thickness, and ϕ is the tunneling barrier height.

In the theoretical fitting, the parameters used are:

LRS: $\phi = 1.7$ eV, $d = 3.00$ nm, and $m^* = 0.3 m_0$;

HRS: $\phi = 1.7$ eV, $d = 3.48$ nm, and $m^* = 0.3 m_0$,

where m_0 is the mass of the electron.

Based on these parameters, the difference between LRS and HRS I - V characteristics can be explained by a 0.48 nm change in the depletion layer width.

1) J. G. Simmons, *J. Appl. Phys.*, 1963, **34**, 1793.

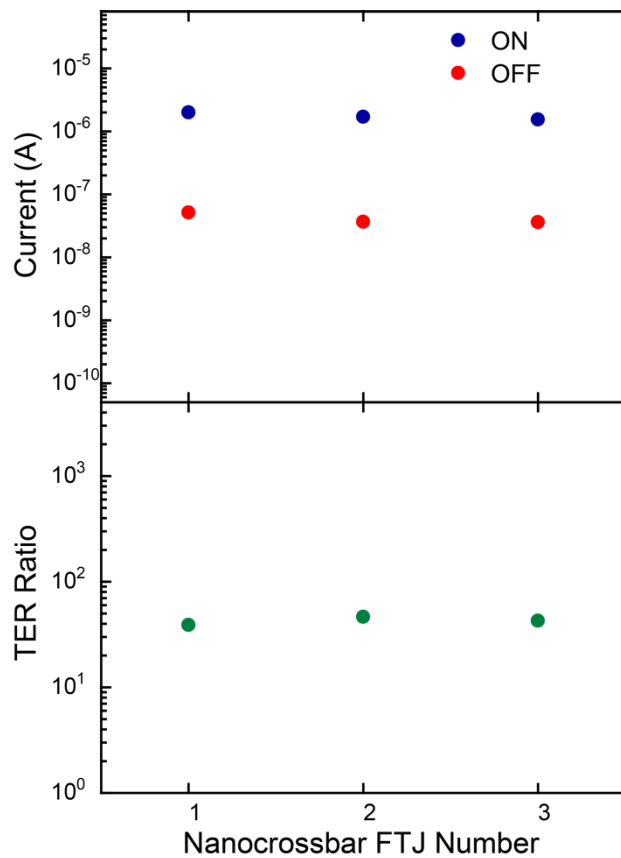


Figure S6. Comparison of ON/OFF currents and TER ratios among nanocrossbar $\text{Ti}/\text{TiO}_x/\text{YHO}_7/\text{Pt}$ FTJs with identical device dimensions. The ON-state current, OFF-state current, and corresponding TER ratios were measured for several $\text{Ti}/\text{TiO}_x/\text{YHO}_7$ (3 nm)/Pt nanocrossbar FTJs with a lateral size of $50 \times 50 \text{ nm}^2$.

All devices exhibit nearly identical ON- and OFF-state current levels and consistent TER ratios within experimental variation, confirming good reproducibility and uniformity of the device performance despite the coexistence of multiple structural phases in the ultrathin YHO_7 films.

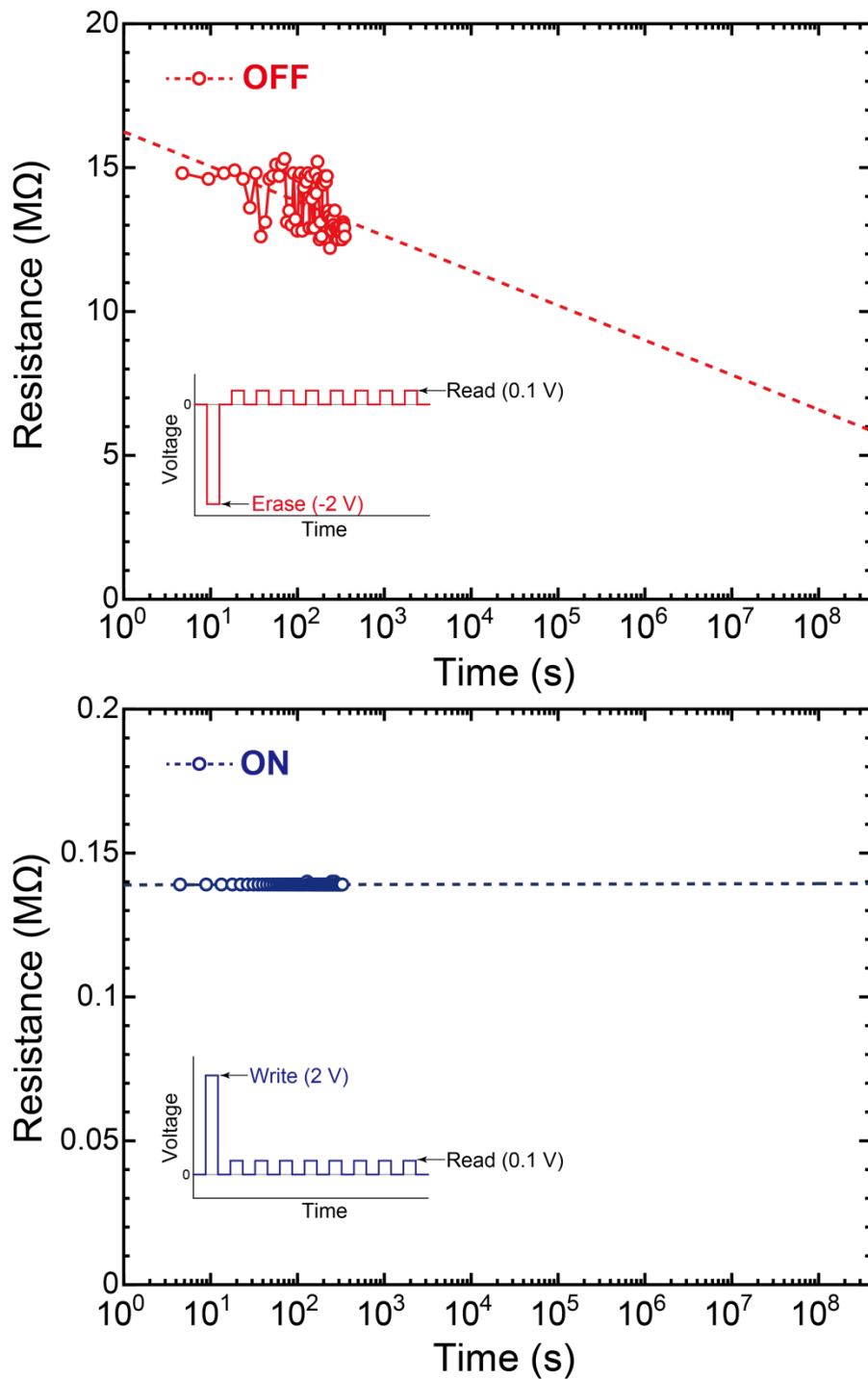


Figure S7. Linear R-log time plots for the data retention characteristics of the nanocrossbar Ti/TiO_x/YHO₇/Pt FTJ. (a) Linear R-log time plot for the OFF state and (b) for the ON state of a 30 × 30 nm² Ti/TiO_x/YHO₇ (3 nm)/Pt nanocrossbar FTJ, derived from the same dataset used in Figure 6 of the manuscript. Each plot shows the resistance (R) as a function of the logarithm of time, measured up to 10³ s. The OFF-state resistance gradually decreases with time, while the ON-state current remains almost unchanged over the entire measurement period.

In the extrapolated linear R-log time plots, the OFF-state resistance—and consequently the TER ratio—are projected to decrease to approximately half of their initial values after 10 years ($\approx 3.15 \times 10^8$ s). Nevertheless, a distinct and durable resistance contrast between the ON and OFF states would remain, demonstrating robust long-term non-volatile functionality of the nanoscale FTJ devices.

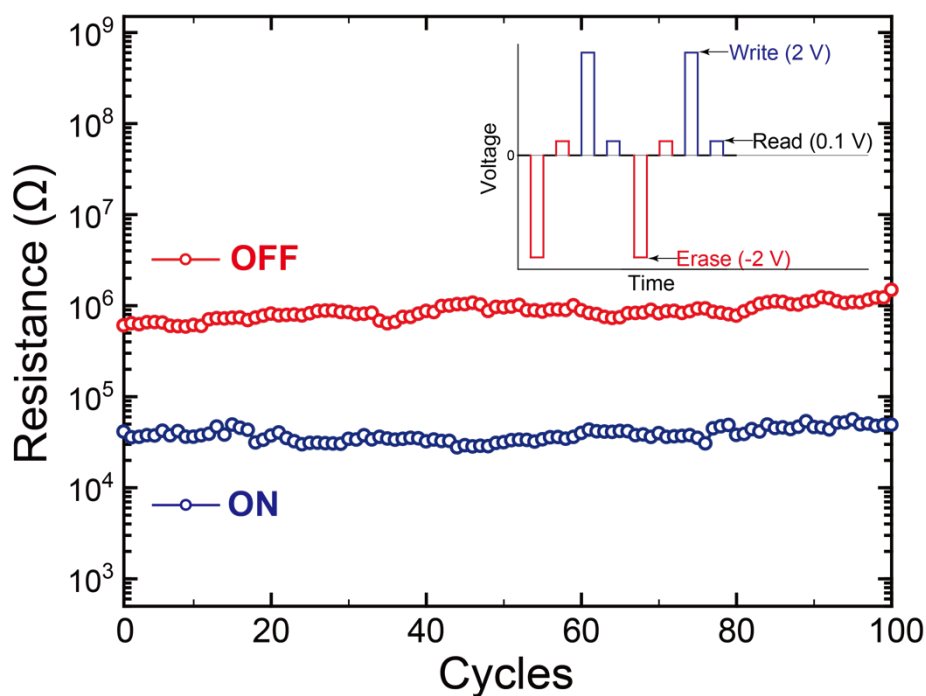


Figure S8. Endurance characteristics of the nanocrossbar $\text{Ti}/\text{TiO}_x/\text{YHO}_7/\text{Pt}$ FTJ.

The resistance values of a $50 \times 50 \text{ nm}^2$ $\text{Ti}/\text{TiO}_x/\text{YHO}_7$ (3 nm)/Pt nanocrossbar FTJ were measured at a read voltage of 0.1 V during 100 successive ON/OFF switching cycles. The device was repeatedly switched by applying write and erase voltages of +2 V and -2 V, respectively. The stable and reproducible resistive switching behavior without noticeable degradation confirms the reliable endurance performance of the $50 \times 50 \text{ nm}^2$ scale nanocrossbar FTJ, demonstrating that the device can withstand at least 100 consecutive switching operations.